

# LENet: Lightweight And Efficient LiDAR Semantic Segmentation Using Multi-Scale Convolution Attention

Ben Ding<sup>1</sup> and Ji-Chao Jiao<sup>2</sup>

**Abstract**—LiDAR semantic segmentation can provide vehicles with a rich understanding of scene, which is essential to the perception system in robotics and autonomous driving. In this paper, we propose LENet, a lightweight and efficient projection-based LiDAR semantic segmentation network, which has an encoder-decoder architecture. The encoder consists of a set of MSCA module, which is a simple convolutional attention module to capture multi-scale feature maps. The decoder consists of IAC module, which uses bilinear interpolation to upsample the multi-resolution feature maps and a single convolution layer to integrate the previous and current dimensional features. IAC is very lightweight and dramatically reduces the complexity and storage cost. Moreover, we introduce multiple auxiliary segmentation heads to further refine the network accuracy. We have conducted detailed quantitative experiments, which shows how each component contributes to the final performance. We evaluate our approach on well known public benchmarks (SemanticKITTI), which demonstrates our proposed LENet is more lightweight and effective than state-of-the-art semantic segmentation approaches. Our full implementation will be available at <https://github.com/fengludb/LENet>.

**Index Terms**—LiDAR point clouds, 3D semantic segmentation, LiDAR perception, Autonomous Driving

## I. INTRODUCTION

Environment perception can help vehicles understand the surrounding scene, which is essential to autonomous driving. LiDAR and RGB cameras are common sensors in the perception system of autonomous driving. Compared to cameras, LiDAR sensor isn't affected by lighting and weather conditions, thus being more robust. Meanwhile, compared to 2D image, LiDAR point cloud can accurately describe the structure of an object, and provide vehicles with a geometry-accurate representation of the surroundings. Therefore 3D point cloud analysis has drawn more and more attention. Especially, point cloud semantic segmentation aims to assign the labels for each point, which helps vehicles gain a rich understanding of the scene. Therefore, point cloud semantic segmentation is becoming an interesting research topic in both academic and industrial communities.

Due to the disorder and irregularity of 3d point cloud, we can't directly perform standard Convolution Neural Networks on it. To tackle the problem, extensive research efforts have been devoted to point cloud semantic segmentation during the past year. Point-based method [2]–[5] directly extract features from the raw point cloud, which can reduce the impact of computational complexity and noise errors in the pre-processing process. However, they usually have high computational complexity and limited processing speed. Voxel-based methods convert the irregular point clouds into regular grid representation so that the 3D convolutional neu-

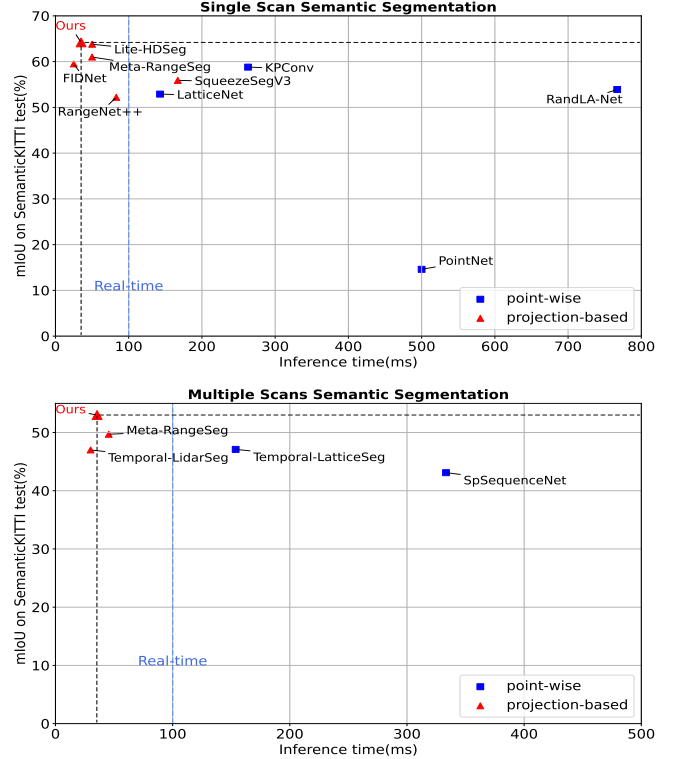


Fig. 1. Accuracy(mIoU) versus inference time. Our presented LENet obtains the promising results on both single scan and multiple scans semantic segmentation in SemanticKITTI test dataset [1].

ral networks can be employed. Although voxel-base methods can achieve the state-of-the-art accuracy, they mainly suffer from heavy computations especially for large-scale LiDAR point clouds in outdoor scenes of autonomous driving. Projection-based methods transform the raw point cloud into an 2D range image by spherical projection strategy. Compared to point-based methods and voxel-based methods, projection-based have a superior inference speed and nice accuracy performance. Meanwhile, they have recently received increasing attention since the great success of fully convolutional networks on image semantic segmentation.

In this work, we presents a lightweight and efficient projection-based LiDAR semantic segmentation network. Experimental results on well known public benchmarks (SemanticKITTI) demonstrates that our network have higher accuracy performance and can run in real time (as shown in Fig. 1) with less parameters than prior works (as shown in table III). In summary, the main contribution of this paper as follows: leftmargin=\*

- We present a simple muti-scale convolutional attention

module (MSCA), which can capture the information of objects with varying size in the full 360 degrees LiDAR scan.

- A novel IAC module, which uses bilinear interpolation to upsample the multi-resolution feature maps and a single convolution layer to integrate the previous and current dimensional feature. IAC is very lightweight and dramatically reduces the complexity and storage cost.
- By introducing multiple auxiliary segmentation heads, we further refine the network accuracy without introducing additional inference parameters.
- We conduct extensive experiments on the publicly available datasets, SemanticKITTI [1]. The results show that our method achieves state-of-the-art performance.

## II. RELATED WORK

With the prevalence a large-scale dataset [1], [6], [7] for the task of point cloud segmentation of autonomous driving scenes and the rapid development of deep learning, a wide range of 3D LiDAR point clouds semantic segmentation methods using deep learning have been proposed over the past years. Generally, they can be broadly categorized into three groups according to the representations of input data, include point, voxel and range map.

**Point-based methods** directly process the raw 3D point cloud without applying any additional transformation or pre-processing, which are able to preserve the 3D spatial structure information. The pioneering methods of this group are PointNet [2] and PointNet++ [3], which use shared MLPs to learn the properties of each point. In subsequent series of works, KPConv [8] develops deformable convolutions that can use arbitrary number of kernel points to learn local geometry. However, these approaches have the disadvantages of high computational complexity and large memory consumption, which hinders them from the large-scale point cloud. RandLA-Net [5] adopts a random sampling strategy and uses local feature aggregation to reduce the information loss caused by random operations, which considerably improve the efficiency of point cloud processing and decrease the use of memory consumption.

**Voxel-based Methods** Voxel-based approach to convert point clouds into voxels for processing, which can effectively solve the irregularity problem. The early voxel-based methods firstly transform a point cloud into 3D voxel representations, then use the standard 3D CNN to predict semantic labels. However, the regular 3D convolution requires the huge memory and heavy computational power. Minkowski [9] CNN chose to use sparse convolution instead of standard 3D convolution and other standard neural network to reduce the computational cost. Cylinder3D [10] adopts 3D space partition and designs an asymmetrical residual block to reduce computation. AF2S3Net [11] achieves state-of-the-art of voxel-methods, which proposes two novel attention blocks name Attentive Feature Fusion Module(AF2M) and Adaptive Feature Fusion(ASFM) to effectively learn local features and global contexts.

**Projection-based Methods** project 3D point clouds into 2D image space, which can take advantage of a large amount of advanced layers for image feature extraction. SqueezeSeg [12] proposes spherical projection which maps the scatter 3D laser points into 2D Range-Image, then uses the lightweight model SqueezeNet and CRF for segmentation. Subsequently, SqueezeSegV2 [13] proposes context aggregation module (CAM) to aggregate contextual information from a larger perceptual field. RangeNet++ [14] integrates Darknet into SqueezeSeg and proposes an efficient KNN post-processing method to predict labels for point. SqueezeSegV3 [15] proposes Spatially-Adaptive Convolution (SAC) with different filters depending on the location of the input image. SalsaNet [16] inherits the encoder-decoder architecture from SalsaNet [17] and presents an uncertainty-aware mechanism for point feature leaning. Lite-HDseg [18] achieves state-of-the-art performance by introducing three different modules, Inception-like Context Module, Multi-class Spatial Propagation Network, and a boundary loss.

## III. METHOD

### A. Range Image Representation.

Using the spherical projection approach, we can transform the unstructured point cloud into an ordered range image representation. The advantages of range representation are that it can use the effective 2D convolutional operation for fast training and inference, and it can facilitate the mature deep learning technologies that have been well studied in image-based tasks.

In the range image representation, each LiDAR point  $p = (x, y, z)$  with Cartesian coordinates, a spherical mapping  $\mathbb{R}^3 \rightarrow \mathbb{R}^2$  is used to transform it to image coordinates, as below:

$$\begin{pmatrix} u \\ v \end{pmatrix} = \begin{pmatrix} \frac{1}{2} [1 - \arctan(y, x) \pi^{-1}] w & \\ [1 - (\arcsin(z r^{-1}) + f_{\text{up}}) f^{-1}] h & \end{pmatrix}, \quad (1)$$

where  $(u, v)$  are image coordinates,  $(h, w)$  are the height and width of the desired range image representation,  $f = f_{\text{up}} + f_{\text{down}}$  is the vertical field-of-view of the sensor, and  $r = \sqrt{x^2 + y^2 + z^2}$  is the range of each point.

### B. Convolution Attention Encoder

Multi-scale features play a significant role in semantic segmentation since semantic segmentation tasks usually need to process objects of different size in a single image. A common approach to extract multi-scale features is to use a combination of a set of convolutions having different receptive fields, then fusing these respective fields, such as [16]. Inspired by SegNext [19], we propose a novel multi-scale convolution attention module (MSCA).

As depicted in Fig.3 (b), MSCA consists of three parts: a depth-wise convolution to aggregate local information, multi-branch depth-wise strip convolutions to capture multi-scale context, and an  $1 \times 1$  convolution to model relationship between different channels. Finally, the output of  $1 \times 1$  convolution is used as attention weights directly to re-weight the input of MSCA. In addition, we adopt the pyramid

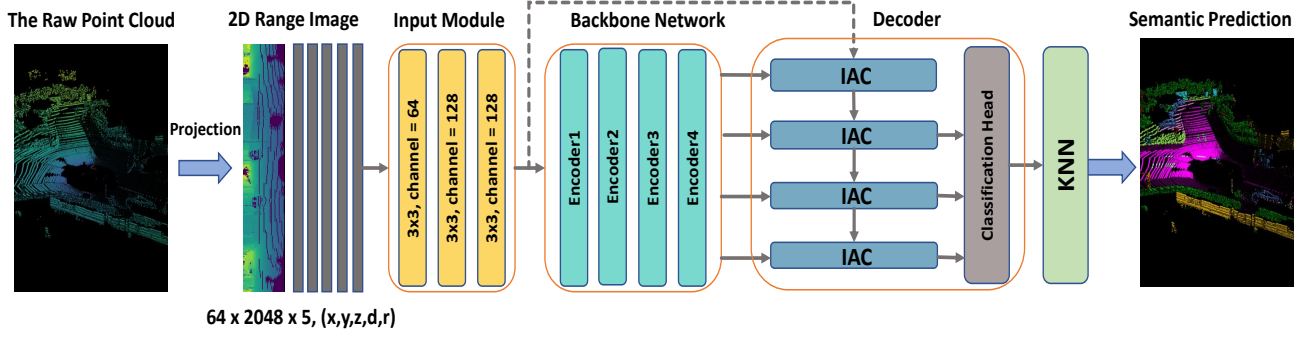


Fig. 2. Illustration of our proposed LENet framework. The backbone network is consisted of MSCA and has the pyramid structure similar to ResNet34. The ICA module upsamples the low-dimensional feature maps to original size and aggregate it with the output of the previous IAC module. Then, the last classification head receives the feature maps from the last three ICA module and outputs the label of each point. Finally, we use K Nearest Neighbors (KNN) to do post-processing.

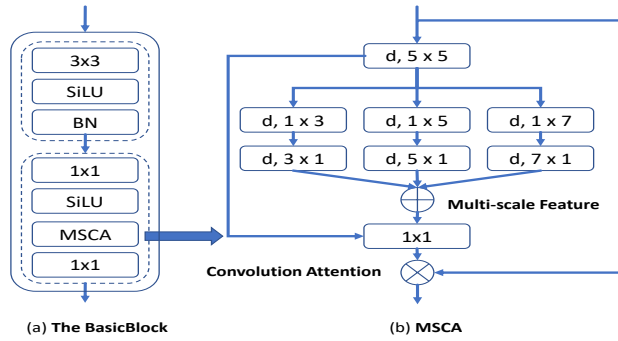


Fig. 3. Illustration of the BasicBlock that is used to build the encoder and the proposed MSCA. Here,  $d$  means a depth-wise convolution,  $k_1 \times k_2$  means the kernel size of the convolution layer. We extract multi-scale features using the convolutions and then utilize them as attention weights to reweight the input of MSCA.

structure for our encoder following [20], [21] and the building block in the encoder is composed with a  $3 \times 3$  convolution layer and MSCA as shown in Fig.3 (a).

### C. IAC Decoder

To design a simple and effective decoder, We investigate several different decoder structure. In [14]–[16], they use standard transpose convolutions or *pixel-shuffle* to produce the upsampled feature maps, then using a set of convolution to decode the feature maps, which is effective but computationally heavy. In FIDNet, it's decoder uses FID (fully interpolation decoding) to decode the semantics of different levels, then using a classification head to fuse these semantics. Although FID is completely parameter-free, it doesn't have the ability to learn from feature, which makes model's performance excessively depend on the classification head. Besides, FIDNet's classification fuse too much low-level information, which hurts the performance.

In this work, we presented a lightweight decoder as depicted in Fig. 2. The IAC module contains two parts: a bilinear interpolation to upsample the feature maps which come from the encoder, a  $3 \times 3$  convolution to fuse the information from the encoder and the previous IAC. Finally, we use the point-wise convolution to fuse the features from

the last three IAC modules. In three different decoder, our decoder has fewest parameters and best performance.

### D. Loss Function

In this work, we train the proposed neural network with three different loss functions, namely weighted cross-entropy loss  $\mathcal{L}_{wce}$ , Lovász loss  $\mathcal{L}_{ls}$  and boundary loss  $\mathcal{L}_{bd}$ . Finally, our total loss is following:

$$\mathcal{L} = w_1 \mathcal{L}_{wce} + w_2 \mathcal{L}_{ls} + w_3 \mathcal{L}_{bd}, \quad (2)$$

$w_1$ ,  $w_2$  and  $w_3$  are the weights with respect to each loss function. In our implementation, we set  $w_1 = 1$ ,  $w_2 = 1.5$  and  $w_3 = 1$ .

Three loss functions account for three different problems. To cope with the imbalanced classes problem, the weighted cross-entropy loss  $\mathcal{L}_{wce}$  [32] is employed to maximize the prediction accuracy for point labels, which is able to balance the distributions among different classes. It's defined as

$$\mathcal{L}_{wce}(y, \hat{y}) = - \sum_i \frac{1}{\sqrt{f_i}} p(y_i) \log(p(\hat{y}_i)), \quad (3)$$

where  $y_i$  represents the ground truth, and  $\hat{y}_i$  is prediction and  $f_i$  is the frequency of the  $i_{th}$  class.

To solve the problem of optimizing the intersection-over-union(IoU), the Lovász loss  $\mathcal{L}_{ls}$  [33] is used to maximize the intersection-over-union (IoU) score that is commonly used to in performance evaluation on semantic segmentation. It's defined as:

$$\mathcal{L}_{ls} = \frac{1}{|C|} \sum_{c \in C} \overline{\Delta_{J_c}}(m(c)), \quad m_i(c) = \begin{cases} 1 - x_i(c) & \text{if } c = y_i(c) \\ x_i(c) & \text{otherwise} \end{cases} \quad (4)$$

where  $|C|$  is the class number,  $\overline{\Delta_{J_c}}$  represents the Lovász extension of the Jaccard index,  $x_i(c) \in [0, 1]$  and  $y_i(c) \in \{-1, 1\}$  hold the predicted probability and ground truth label of pixel  $i$  for class  $c$ , respectively.

To account for the blurred segmentation boundaries problem as suggested in [18], [28], [35], the boundary loss function  $\mathcal{L}_{bd}$  [34] is used for LiDAR semantic segmentation, which can be formulated defined as follows:

$$\mathcal{L}_{bd}(y, \hat{y}) = 1 - \frac{2P_b^c R_b^c}{P_b^c + R_b^c}, \quad (5)$$

TABLE I  
THE PERFORMANCE COMPARISON ON SEMANTICKITTI MULTIPLE SINGLE SCAN BENCHMARK.

Methods	Size	mean-IoU	FPS (Hz)	car	bicycle	motorcycle	truck	other-vehicle	person	bicyclist	motorcyclist	road	parking	sidewalk	other-ground	building	fence	vegetation	trunk	terrain	pole	traffic-sign
PointNet [2]	50K pts	14.6	2	46.3	1.3	0.3	0.1	0.8	0.2	0.2	0.0	61.6	15.8	35.7	1.4	41.4	12.9	31.0	4.6	17.6	2.4	3.7
PointNet++ [3]	50K pts	20.1	0.1	53.7	1.9	0.2	0.9	0.2	0.9	1.0	0.0	72.0	18.7	41.8	5.6	62.3	16.9	46.5	13.8	30.0	6.0	8.9
SPLATNet [22]	50K pts	22.8	1	66.6	0.0	0.0	0.0	0.0	0.0	0.0	0.0	70.4	0.8	41.5	0.0	68.7	27.8	72.3	35.9	35.8	13.8	0.0
TangentConv [23]	50K pts	35.9	0.3	86.8	1.3	12.7	11.6	10.2	17.1	20.2	0.5	82.9	15.2	61.7	9.0	82.8	44.2	75.5	42.5	55.5	30.2	22.2
LatticeNet [24]	50K pts	52.9	7	92.9	16.6	22.2	26.6	21.4	35.6	43.0	46.0	90.0	59.4	74.1	22.0	88.2	58.8	81.7	63.6	63.1	51.9	48.4
RandLA-Net [5]	50K pts	53.9	1.3	94.2	26.0	25.8	40.1	38.9	49.2	48.2	7.2	90.7	60.3	73.7	20.4	86.9	56.3	81.4	61.3	66.8	49.2	47.7
KPConv [8]	50K pts	58.8	3.8	<b>96.0</b>	30.2	42.5	33.4	44.3	61.5	61.6	11.8	88.8	61.3	72.7	31.6	90.5	64.2	<b>84.8</b>	69.2	<b>69.1</b>	56.4	47.4
BAAF-Net [25]	50K pts	59.9	4.8	95.4	31.8	35.5	<b>48.7</b>	<b>46.7</b>	49.5	55.7	33.0	90.9	62.2	74.4	23.6	89.8	60.8	82.7	63.4	67.9	53.7	52.0
RangeNet53++ [14]	64 × 2048	52.2	12	91.4	25.7	34.4	25.7	23.0	38.3	38.8	4.8	91.8	65.0	75.2	27.8	87.4	58.6	80.5	55.1	64.6	47.9	55.9
MINet [26]	64 × 2048	55.2	24	90.1	41.8	34.0	29.9	23.6	51.4	52.4	25.0	90.5	59.0	72.6	25.8	85.6	52.3	81.1	58.1	66.1	49.0	59.9
3D-MiniNet [27]	64 × 2048	55.8	28	90.5	42.3	42.1	28.5	29.4	47.8	44.1	14.5	91.6	64.2	74.5	25.4	89.4	60.8	82.8	60.8	66.7	48.0	56.6
SqueezeSegV3 [15]	64 × 2048	55.9	6	92.5	38.7	36.5	29.6	33.0	45.6	46.2	20.1	91.7	63.4	74.8	26.4	89.0	59.4	82.0	58.7	65.4	49.6	58.9
SalsaNext [16]	64 × 2048	59.5	24	91.9	48.3	38.6	38.9	31.9	60.2	59.0	19.4	91.7	63.7	75.8	29.1	90.2	64.2	81.8	63.6	66.5	54.3	62.1
FIDNet [21]	64 × 2048	59.5	<b>29</b>	93.9	54.7	48.9	27.6	23.9	62.3	59.8	23.7	90.6	59.1	75.8	26.7	88.9	60.5	84.5	64.4	69.0	53.3	62.8
Meta-RangeSeg [28]	64 × 2048	61.0	26	93.9	50.1	43.8	43.9	43.2	63.7	53.1	18.7	90.6	64.3	74.6	29.2	91.1	64.7	82.6	65.5	65.5	56.3	64.2
Lite-HDseg [18]	64 × 2048	<b>63.8</b>	20	92.3	40.0	<b>55.4</b>	37.7	39.6	59.2	<b>71.6</b>	<b>54.1</b>	<b>93.0</b>	68.2	<b>78.3</b>	29.3	91.5	65.0	78.2	65.8	65.1	59.5	<b>67.7</b>
LENet(Ours)	64 × 2048	<b>64.2</b>	26	93.9	<b>55.7</b>	48.6	40.1	44.0	<b>67.4</b>	64.4	27.7	92.4	<b>68.8</b>	78.2	<b>32.3</b>	<b>92.1</b>	<b>68.8</b>	84.5	<b>69.4</b>	<b>69.1</b>	<b>59.7</b>	62.4

TABLE II  
THE PERFORMANCE COMPARISON ON SEMANTICKITTI MULTIPLE SCANS BENCHMARK. THE ITEM WITH ARROW INDICATES THE MOVING CLASS

Methods	mean-IoU	FPS (Hz)	car	bicycle	motorcycle	truck	other-vehicle	person	bicyclist	motorcyclist	road	parking	sidewalk	other-ground	building	fence	vegetation	trunk	terrain	pole	traffic sign	car↑	bicyclist↑	person↑	motorcyclist↑	other-vehicle↑	truck↑
TangentConv [23]	34.1	-	84.9	2.0	18.2	21.1	18.5	1.6	0.0	0.0	83.9	38.3	64.0	15.3	85.8	49.1	79.5	43.2	56.7	36.4	31.2	40.3	1.1	6.4	1.9	<b>30.1</b>	<b>42.2</b>
DarkNet53Seg [1]	41.6	-	84.1	30.4	32.9	20.2	20.7	7.5	0.0	0.0	91.6	64.9	75.3	27.5	85.2	56.5	78.4	50.7	64.8	38.1	53.3	61.5	14.1	15.2	0.2	28.9	37.8
SpSequenceNet [29]	43.1	3	88.5	24.0	26.2	29.2	22.7	6.3	0.0	0.0	90.1	57.6	73.9	27.1	<b>91.2</b>	<b>66.8</b>	84.0	66.0	65.7	50.8	48.7	53.2	41.2	26.2	36.2	2.3	0.1
TemporalLidarSeg [30]	47.0	30	92.1	47.7	40.9	<b>39.2</b>	35.0	14.4	0.0	0.0	91.8	59.6	75.8	23.2	89.8	63.8	82.3	62.5	64.7	52.6	60.4	68.2	42.8	40.4	12.9	12.4	2.1
TemporalLatticeNet [31]	47.1	6.5	91.6	35.4	36.1	26.9	23.0	9.4	0.0	0.0	91.5	59.3	75.3	27.5	89.6	65.3	<b>84.6</b>	66.7	<b>70.4</b>	57.2	60.4	59.7	41.7	9.4	<b>48.8</b>	5.9	0.0
Meta-RangeSeg [28]	49.7	22	90.8	50.0	49.5	29.5	34.8	16.6	0.0	0.0	90.8	62.9	74.8	26.5	89.8	62.1	82.8	65.7	66.5	56.2	<b>64.5</b>	69.0	60.4	57.9	22.0	16.6	2.6
LENet(Ours)	<b>53.0</b>	<b>25.3</b>	<b>92.4</b>	<b>57.0</b>	<b>52.1</b>	38.5	<b>47.0</b>	<b>19.0</b>	0.0	<b>4.3</b>	<b>92.0</b>	<b>68.6</b>	<b>77.3</b>	<b>29.9</b>	90.2	63.4	83.4	<b>68.1</b>	67.6	<b>58.0</b>	62.9	<b>75.2</b>	<b>65.2</b>	<b>62.6</b>	22.5	25.7	2.0

where  $P_b^c$  and  $R_b^c$  define the precision and recall of predicted boundary image  $\hat{y}^b$  to real one  $y^b$  for class  $c$ . The boundary image is computed as follows:

$$\begin{aligned} y^b &= \text{pool}(1 - y, \theta_0) - (1 - y) \\ \hat{y}^b &= \text{pool}(1 - \hat{y}, \theta_0) - (1 - \hat{y}) \end{aligned} \quad (6)$$

where  $\text{pool}(\cdot, \cdot)$  employs a pixel-wise max-pooling on a sliding window of size  $\theta_0$ . In addition, we set  $\theta_0 = 3$ .

In our proposed network, the classification head fusions the last three different dimensional feature map to conduct the output, which causes its performance relies heavily on the last three IAC module. Therefore, we use the auxiliary segmentation head to further refine our proposed network accuracy. These auxiliary segmentation heads compute the weighted loss together with the main loss. Meanwhile, each loss has the corresponding weight since the different dimensional feature maps have different expressive power, which is different from [15], [35]. The final loss function can be defined as,

$$L_{total} = L_{main} + \sum_{i=1}^3 \lambda_i L(y_i, \hat{y}_i) \quad (7)$$

where  $L_{main}$  is the main loss,  $y_i$  is the semantic output obtained from stage  $i$ , and  $\hat{y}_i$  represents the corresponding semantic label.  $L(\cdot)$  is computed according to Equation 2. In

our implementation, we set  $\lambda_1 = 1$ ,  $\lambda_2 = 1$  and  $\lambda_3 = 0.5$ , empirically.

#### E. Implementation details.

We use PyTorch [36] to implement our method and do all experiments on a PC with 4 NVIDIA RTX 3090 GPUs. We train network for 50 epochs with initial learning rate  $2e^{-3}$ , which is dynamically adjusted by a cosine annealing scheduler [37]. The batch size is set to 8, the height and width of the range image are set to  $H = 64$  and  $W = 2048$ , respectively. The optimizer is AdamW [38] with the default configuration in Pytorch. During training process, we adopt random rotation, random point dropout, and flipping the 3D point cloud to perform data augmentation.

### IV. EXPERIMENT

#### A. Experiment Setups

**Datasets.** We train and evaluate our network on SemanticKITTI dataset, which is a large-scale dataset for the task of point cloud segmentation of autonomous driving scenes. It provides the dense point-wise annotation for 22 sequences (43,551 scans) in KITTI Odometry [39] Benchmark. Sequence 00 to 10 (19,130 scans) are used for training, 11 to 21 (20,351 scans) for testing. We follow the setting in [1], and use sequence 08 (4,071 scans) for validation. To evaluate



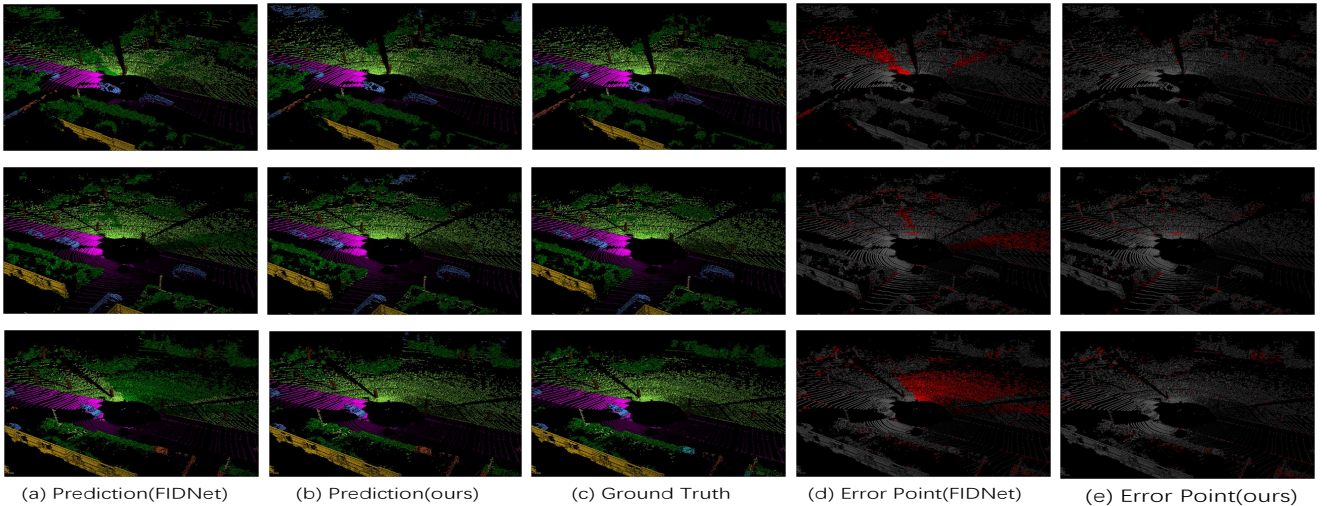


Fig. 4. Qualitative analysis on the SemanticKITTI validation set (sequence 08). Where (a) and (b) are the predictions of FIDNet and our method respectively, (c) is the semantic segmentation ground truth, (d) and (e) are segmentation error maps of FIDNet and our methods, where red indicates wrong prediction.

TABLE III

ABLATION STUDY EVALUATED ON SEMANTICKITTI VALIDATION SET.

Baseline	Row	MSCA	IAC	Boundary Loss	Auxiliary Loss	mIoU	Params(M)
Baseline	1	✗	✗	✗	✗	58.3	6.05
Ours	2	✓	✗	✗	✗	59.3	5.28
	3	✓	✓	✗	✗	59.9	4.74
	4	✓	✓	✓	✗	61.1	4.74
	5	✓	✓	✓	✓	63.1	4.74

the effectiveness of our proposed approach, we submit the output the online evaluation website to obtain the results on the testing set.

**Evaluation Metrics.** To facilitate the fair comparison, we evaluate the performance of different methods with respect to the mean intersection over union metric (mIoU), which is defined as below:

$$\text{mIoU} = \frac{1}{n} \sum_{c=1}^n \frac{\text{TP}_c}{\text{TP}_c + \text{FP}_c + \text{FN}_c}, \quad (8)$$

where  $\text{TP}_c$ ,  $\text{FP}_c$ , and  $\text{FN}_c$  represent true positive, false positive, and false negative predictions for the class  $c$ .

### B. Evaluation Results and Comparisons

Table I and Table II show the quantitative results of recent available and published methods on SemanticKITTI single scan benchmark and multiple scans benchmark, respectively. It can be seen from tables that our presented method achieves the state-of-the-art performance compared to point-based and image-based on both the single scan benchmark (64.2% mIoU) and multiple scan benchmark (53.0% mIoU). Meanwhile, it's worthy of mentioning that our proposed network is very lightweight with around 4.7 M parameters and fast with 26FPS while maintaining high accuracy.

To better visualize the improvements of our proposed model over the baseline, we provide the qualitative comparison exaples in Fig. 4, where we compare FIDNet and LENet in terms of the prediction result and the generated error map in three data frames. It can be seen that our presented method has a significant improvement over FIDNet.

### C. Ablation Studies

In this section, we conducted several ablation experiments on the SemanticKITTI validation set (sequence 08) to examine the improvement of each individual module in our proposed network. For the validation of each setup, the size of input range image is  $64 \times 2048$ , the channel of input range image is 5. Table III shows the total number

of model parameters with the corresponding mIoU scores on the SemanticKITTI validation set.

For fair comparison, we firstly treat FIDNet the baseline method, which has the similar network structure as ours. Next, we replace the baseline with proposed MSCA and ICA in Section III. Finally, we add the boundary loss and auxiliary loss one by one, to examine the their effectiveness for our network. As shown in Table III, our network obtains over 1.0% improvement in accuracy when replacing the basic block of baseline, which demonstrates that the multi-scale convolution attention is effective. Next, IAC performs better than the network around 1.0% after replacing the original decoder. Additionally, the boundary loss achieves over 1.2% performance gain and the auxiliary loss gain over 2.0% performance jump. Finally, our presented LENet approach has over 4.8% improvement and decreases around 25% parameters comparing to the baseline, which demonstrate the efficacy of each module.

## V. CONCLUSIONS

In this paper, We presented LENet, a lightweight and efficient real-time CNN model for LiDAR point cloud segmentation task. Firstly, We uses encoder based on multi-scale convolution attention module to better capture the features of objects with varying size in LiDAR data. Then, We propose a simple and effective decoder for upsampling, which significantly reduces the complexity and storage cost. Finally, We trained our network with embed multiple auxiliary segmentation heads to further improve the power of learned feature without introduction of parameters and efficiency cost. The evaluations on the SemanticKITTI test

dataset demonstrate that our proposed method achieves the state-of-the-art performance on both single scan and multiple scans semantic segmentation.

## REFERENCES

- [1] J. Behley, M. Garbade, A. Milioto, J. Quenzel, S. Behnke, C. Stachniss, and J. Gall, "Semantickitti: A dataset for semantic scene understanding of lidar sequences," in *Proceedings of the IEEE/CVF International Conference on Computer Vision*, 2019, pp. 9297–9307.
- [2] C. R. Qi, H. Su, K. Mo, and L. J. Guibas, "Pointnet: Deep learning on point sets for 3d classification and segmentation," in *Proceedings of the IEEE conference on computer vision and pattern recognition*, 2017, pp. 652–660.
- [3] C. R. Qi, L. Yi, H. Su, and L. J. Guibas, "Pointnet++: Deep hierarchical feature learning on point sets in a metric space," *arXiv preprint arXiv:1706.02413*, 2017.
- [4] Y. Li, R. Bu, M. Sun, W. Wu, X. Di, and B. Chen, "Pointcnn: Convolution on  $\chi$ -transformed points," in *Proceedings of the 32nd International Conference on Neural Information Processing Systems*, 2018, pp. 828–838.
- [5] Q. Hu, B. Yang, L. Xie, S. Rosa, Y. Guo, Z. Wang, N. Trigoni, and A. Markham, "Randla-net: Efficient semantic segmentation of large-scale point clouds," in *Proceedings of the IEEE/CVF Conference on Computer Vision and Pattern Recognition*, 2020, pp. 11 108–11 117.
- [6] H. Caesar, V. Bankiti, A. H. Lang, S. Vora, V. E. Liong, Q. Xu, A. Krishnan, Y. Pan, G. Baldan, and O. Beijbom, "nuscenes: A multimodal dataset for autonomous driving," *arXiv preprint arXiv:1903.11027*, 2019.
- [7] Y. Pan, B. Gao, J. Mei, S. Geng, C. Li, and H. Zhao, "Semanticpos: A point cloud dataset with large quantity of dynamic instances," in *2020 IEEE Intelligent Vehicles Symposium (IV)*. IEEE, 2020, pp. 687–693.
- [8] H. Thomas, C. R. Qi, J.-E. Deschaud, B. Marcotegui, F. Goulette, and L. J. Guibas, "Kpconv: Flexible and deformable convolution for point clouds," in *Proceedings of the IEEE/CVF International Conference on Computer Vision*, 2019, pp. 6411–6420.
- [9] C. Choy, J. Gwak, and S. Savarese, "4d spatio-temporal convnets: Minkowski convolutional neural networks," in *Proceedings of the IEEE/CVF Conference on Computer Vision and Pattern Recognition*, 2019, pp. 3075–3084.
- [10] X. Zhu, H. Zhou, T. Wang, F. Hong, Y. Ma, W. Li, H. Li, and D. Lin, "Cylindrical and asymmetrical 3d convolution networks for lidar segmentation," *arXiv preprint arXiv:2011.10033*, 2020.
- [11] R. Cheng, R. Razani, E. Taghavi, E. Li, and B. Liu, "s2-net: Attentive feature fusion with adaptive feature selection for sparse semantic segmentation network," *arXiv preprint arXiv:2102.04530*, 2021.
- [12] B. Wu, A. Wan, X. Yue, and K. Keutzer, "Squeezeseg: Convolutional neural nets with recurrent crf for real-time road-object segmentation from 3d lidar point cloud," in *2018 IEEE International Conference on Robotics and Automation (ICRA)*. IEEE, 2018, pp. 1887–1893.
- [13] B. Wu, X. Zhou, S. Zhao, X. Yue, and K. Keutzer, "Squeezesegv2: Improved model structure and unsupervised domain adaptation for road-object segmentation from a lidar point cloud," in *2019 International Conference on Robotics and Automation (ICRA)*. IEEE, 2019, pp. 4376–4382.
- [14] A. Milioto, I. Vizzo, J. Behley, and C. Stachniss, "Rangenet++: Fast and accurate lidar semantic segmentation," in *2019 IEEE/RSJ International Conference on Intelligent Robots and Systems (IROS)*. IEEE, 2019, pp. 4213–4220.
- [15] C. Xu, B. Wu, Z. Wang, W. Zhan, P. Vajda, K. Keutzer, and M. Tomizuka, "Squeezesegv3: Spatially-adaptive convolution for efficient point-cloud segmentation," in *European Conference on Computer Vision*. Springer, 2020, pp. 1–19.
- [16] T. Cortinhal, G. Tzelepis, and E. E. Aksoy, "Salsanet: Fast semantic segmentation of lidar point clouds for autonomous driving," *arXiv preprint arXiv:2003.03653*, 2020.
- [17] E. E. Aksoy, S. Baci, and S. Cavdar, "Salsanet: Fast road and vehicle segmentation in lidar point clouds for autonomous driving," in *2020 IEEE Intelligent Vehicles Symposium (IV)*. IEEE, 2019, pp. 926–932.
- [18] R. Razani, R. Cheng, E. Taghavi, and L. Bingbing, "Lite-hdseg: Lidar semantic segmentation using lite harmonic dense convolutions," in *2021 IEEE International Conference on Robotics and Automation (ICRA)*. IEEE, 2021, pp. 9550–9556.
- [19] M.-H. Guo, C.-Z. Lu, Q. Hou, Z. Liu, M.-M. Cheng, and S.-M. Hu, "Segnext: Rethinking convolutional attention design for semantic segmentation," *arXiv preprint arXiv:2209.08575*, 2022.
- [20] K. He, X. Zhang, S. Ren, and J. Sun, "Deep residual learning for image recognition," in *Proceedings of the IEEE conference on computer vision and pattern recognition*, 2016, pp. 770–778.
- [21] Y. Zhao, L. Bai, and X. Huang, "Fidnet: Lidar point cloud semantic segmentation with fully interpolation decoding," in *2021 IEEE/RSJ International Conference on Intelligent Robots and Systems (IROS)*. IEEE, 2021, pp. 4453–4458.
- [22] H. Su, V. Jampani, D. Sun, S. Maji, E. Kalogerakis, M.-H. Yang, and J. Kautz, "Splatnet: Sparse lattice networks for point cloud processing," in *Proceedings of the IEEE conference on computer vision and pattern recognition*, 2018, pp. 2530–2539.
- [23] M. Tatarchenko, J. Park, V. Koltun, and Q.-Y. Zhou, "Tangent convolutions for dense prediction in 3d," in *Proceedings of the IEEE Conference on Computer Vision and Pattern Recognition*, 2018, pp. 3887–3896.
- [24] R. A. Rosu, P. Schütt, J. Quenzel, and S. Behnke, "Latticenet: Fast point cloud segmentation using permutohedral lattices," *arXiv preprint arXiv:1912.05905*, 2019.
- [25] S. Qiu, S. Anwar, and N. Barnes, "Semantic segmentation for real point cloud scenes via bilateral augmentation and adaptive fusion," in *Proceedings of the IEEE/CVF Conference on Computer Vision and Pattern Recognition*, 2021, pp. 1757–1767.
- [26] S. Li, X. Chen, Y. Liu, D. Dai, C. Stachniss, and J. Gall, "Multi-scale interaction for real-time lidar data segmentation on an embedded platform," *IEEE Robotics and Automation Letters*, vol. 7, no. 2, pp. 738–745, 2021.
- [27] I. Alonso, L. Riazuelo, L. Montesano, and A. C. Murillo, "3d-mininet: Learning a 2d representation from point clouds for fast and efficient 3d lidar semantic segmentation," *IEEE Robotics and Automation Letters*, vol. 5, no. 4, pp. 5432–5439, 2020.
- [28] S. Wang, J. Zhu, and R. Zhang, "Meta-rangeseg: Lidar sequence semantic segmentation using multiple feature aggregation," *arXiv preprint arXiv:2202.13377*, 2022.
- [29] H. Shi, G. Lin, H. Wang, T.-Y. Hung, and Z. Wang, "Spsequencenet: Semantic segmentation network on 4d point clouds," in *Proceedings of the IEEE/CVF conference on computer vision and pattern recognition*, 2020, pp. 4574–4583.
- [30] F. Duerr, M. Pfaller, H. Weigel, and J. Beyerer, "Lidar-based recurrent 3d semantic segmentation with temporal memory alignment," in *2020 International Conference on 3D Vision (3DV)*. IEEE, 2020, pp. 781–790.
- [31] P. Schutt, R. A. Rosu, and S. Behnke, "Abstract flow for temporal semantic segmentation on the permutohedral lattice," in *2022 International Conference on Robotics and Automation (ICRA)*. IEEE, 2022, pp. 5139–5145.
- [32] Z. Zhang and M. R. Sabuncu, "Generalized cross entropy loss for training deep neural networks with noisy labels," *arXiv preprint arXiv:1805.07836*, 2018.
- [33] M. Berman, A. R. Triki, and M. B. Blaschko, "The lovász-softmax loss: A tractable surrogate for the optimization of the intersection-over-union measure in neural networks," in *Proceedings of the IEEE Conference on Computer Vision and Pattern Recognition*, 2018, pp. 4413–4421.
- [34] H. Kervade, J. Bouchtiba, C. Desrosiers, E. Granger, J. Dolz, and I. B. Ayed, "Boundary loss for highly unbalanced segmentation," in *International conference on medical imaging with deep learning*. PMLR, 2019, pp. 285–296.
- [35] H.-X. Cheng, X.-F. Han, and G.-Q. Xiao, "Cenet: Toward concise and efficient lidar semantic segmentation for autonomous driving," in *2022 IEEE International Conference on Multimedia and Expo (ICME)*. IEEE, 2022, pp. 01–06.
- [36] A. Paszke, S. Gross, S. Chintala, G. Chanan, E. Yang, Z. DeVito, Z. Lin, A. Desmaison, L. Antiga, and A. Lerer, "Automatic differentiation in pytorch," 2017.
- [37] I. Loshchilov and F. Hutter, "Sgdr: Stochastic gradient descent with warm restarts," *arXiv preprint arXiv:1608.03983*, 2016.
- [38] —, "Decoupled weight decay regularization," *arXiv preprint arXiv:1711.05101*, 2017.
- [39] A. Geiger, P. Lenz, and R. Urtasun, "Are we ready for autonomous driving? the kitti vision benchmark suite," in *2012 IEEE conference on computer vision and pattern recognition*. IEEE, 2012, pp. 3354–3361.